ESANN 2023 proceedings, European Symposium on Artificial Neural Networks, Computational Intelligence and Machine Learning. Bruges (Belgium) and online event, 4-6 October 2023, i6doc.com publ., ISBN 978-2-87587-088-9. Available from http://www.i6doc.com/en/.

An Alternating Minimization Algorithm with Trajectory for Direct Exoplanet Detection

Hazan Daglayan[1], Simon Vary[1], and P.-A. Absil[1] *

1- ICTEAM Institute, UCLouvain, 1348 Louvain-la-Neuve, Belgium

Abstract. Effective image post-processing algorithms are vital for the successful direct imaging of exoplanets. Existing algorithms use techniques based on a low-rank approximation to separate the rotating planet signal from the quasi-static speckles. In this paper, we present a novel approach that iteratively finds the planet's flux and the low-rank approximation of quasi-static signals, strengthening the existing model based on low-rank approximations. We implement the algorithm with two different norms and test it on data, showing improvement over classical low-rank approaches. Our results highlight the benefits of iterative refinement of low-rank approximation to enhance planet detection.

1 Introduction

Although significant progress has been made in the field of high-contrast imaging (HCI), including overcoming image degradation caused by the Earth's atmosphere utilizing techniques such as adaptive optics used during observations, only around 1% of the discovered planets have been imaged directly [1]. Dedicated HCI instruments, such as VLT/SPHERE, images of which we use to test algorithms presented in this work, also utilize state-of-the-art coronagraphs to block out the starlight and reduce the contrast between a host star and planet [2]. Despite advances in imaging technology, the noises called *speckles*, which occur in the images because of the imperfections within the telescope and instrument, as well as atmospheric turbulence [3], resemble the signal of the exoplanet in terms of shape and contrast. Therefore, post-processing algorithms are needed to distinguish planets from speckles.

Different observing strategies, such as *angular differential imaging* (ADI) [4], have been proposed to help algorithms separate the exoplanets from the speckles. This approach relies on data gathered through pupil tracking, where the star remains fixed at the center of the images while the Earth rotates during a night. This causes the exoplanet to appear to orbit around its host star over time, while the star and speckles are quasi-static in the images. The ADI technique aims to create a reference point spread function (PSF) that mimics the quasi-static speckle noise in the images. This model of quasi-static speckle noise is then subtracted from the image, the residual is then derotated and combined to enhance the potential exoplanet signal.

A considerable amount of ADI studies aim to solve this problem using low-rank approximation. The widely adopted technique for background subtraction

*This work was supported by the Fonds de la Recherche Scientifique-FNRS under Grant no T.0001.23. Simon Vary is a beneficiary of the FSR Incoming Post-doctoral Fellowship.

ESANN 2023 proceedings, European Symposium on Artificial Neural Networks, Computational Intelligence and Machine Learning. Bruges (Belgium) and online event, 4-6 October 2023, i6doc.com publ., ISBN 978-2-87587-088-9. Available from http://www.i6doc.com/en/.

relies on a low-rank matrix model based on PCA [5, 6]. A variation known as Annular PCA [7, 8] considers only a selected set of pixels within a specified annulus. In these methods, the residual of the least-squares problem captures the rotating planet signal, while the low-rank component accounts for the quasi-static speckles. Building upon this, the LLSG method [9] extends the model by incorporating a sparse matrix term to enhance the accuracy of rotating planet signal capture. The sparse term has been further refined with a trajectory specified by the LRPT method [10]. Recently, a novel approach utilizing an ℓ_1 norm for low-rank approximation has been proposed [11]. Another approach, the Regime-switching model [12], combines multiple advantages of low-rank approximation based PSF subtraction techniques.

In this work, we propose a new method, dubbed Alternating Minimization Algorithm with Trajectory (AMAT), that makes a more advanced use of the low-rank-plus-trajectory model by alternating between computing the low-rank approximation of the speckle field and the planet flux. We pose our model as ℓ_1 and ℓ_2 norm minimization problems. Numerical experiments performed on dataset VLT/SPHERE-IRDIS 51 Eri show the potential of AMAT to improve upon the existing approaches in terms of more clear detections and receiver operating characteristic (ROC) curves.

2 Alternating Minimization Algorithm with Trajectory

Let $M \in \mathbb{R}^{T\times N^2}$ be an ADI sequence that consists of T unfolded images with size $N \times N$. The standard low-rank model [13] can be expressed as

$$M = L + a_g P_g + E, \quad \text{rank}(L) \leq r, \quad P_g \in \Lambda, \tag{1}$$

where L is a low-rank matrix representing the background with quasi-static speckles, a_g, referred to as *flux*, corresponds to the intensity coefficient of the planet signature $P_g \in \Lambda \subset \mathbb{R}^{T\times N^2}$, where $g \in [N] \times [N]$ stands for the position of the planet on the initial frame, Λ is the set of all feasible planet signatures, and E is the noise term.

In existing approaches, the low-rank matrix L is estimated first. In particular, the PCA approach computes L in (1) by truncated SVD. As an alternative, L can be obtained by L1 low-rank approximation (L1-LRA), as proposed in [11]. Once L is estimated, a residual cube is then obtained as $M - L$, from which the planet flux a_g is estimated for each planet trajectory g by various methods; see, e.g., [5, 6, 13].

Instead of sequentially estimating first the component L followed by estimating the flux a_g, we propose to estimate them simultaneously in the following optimization problem

$$\min_{L\in\mathbb{R}^{T\times N^2}, a_g\in\mathbb{R}} \|M - L - a_g P_g\| \quad \text{s.t.} \quad \text{rank}(L) \leq r, \quad P_g \in \Lambda \tag{2}$$

where $\|\cdot\|$ denotes either ℓ_1 or ℓ_2 norm depending on the assumed distribution of the error E in (1). The optimization problem (2) is addressed by alternatingly solving the following two sub-problems until a stopping criterion is met:

ESANN 2023 proceedings, European Symposium on Artificial Neural Networks, Computational Intelligence and Machine Learning. Bruges (Belgium) and online event, 4-6 October 2023, i6doc.com publ., ISBN 978-2-87587-088-9. Available from http://www.i6doc.com/en/.

$$L^{(i)} = \underset{L \in \mathbb{R}^{T \times N^2}}{\operatorname{argmin}} \|M - L - a_g^{(i-1)} P_g\| \tag{3}$$

$$a_g^{(i)} = \underset{a_g \in \mathbb{R}}{\operatorname{argmin}} \|M - L^{(i)} - a_g P_g\|. \tag{4}$$

When the norm is ℓ_2, the matrix $L^{(i)}$ can be obtained by truncated SVD of $M - a_g^{(i-1)} P_g$. The optimal value of $a_g^{(i)}$ can be computed analytically as

$$a_g^{(i)} = \frac{\langle P_g, M - L^{(i)} \rangle}{\|P_g\|_F^2}, \tag{5}$$

where $\langle \cdot, \cdot \rangle$ denotes the Frobenius inner product.

When the norm is ℓ_1, we solve the problem (3) with an algorithm suggested by [11] using an exact block cyclic coordinate descent method. Moreover, (4) becomes a least absolute deviation problem which we solve by an efficient exhaustive search over the kink points of the piecewise linear objective function as in [13].

We produce a flux map, consisting of all possible trajectories, $g \mapsto a_g$ by simply returning (4) in the final iterate of the alternating iteration, then compute the SNR map with VIP [7, 8] and use this as the detection map.

3 Numerical Experiments

We apply our algorithm to the publicly available ADI data set VLT/SPHERE-IRDIS 51 Eri in the K1 (2.11 μm) band with a known planet. The cube has 256 frames covering 42° of parallactic angles and the frames are cropped to 100 by 100 pixels.

We compare our algorithm with the results of the classical PCA approach (annular version) and the results of our algorithm using only a single iteration. Our comparison focuses on the visual quality of the SNR maps [14] with the SNR values on the selected pixels and the ROC curves. We use the same rank parameter $r = 20$ for each algorithm, which was observed to work well for the dataset [12]. In our preliminary experiments, we simply stop the algorithm after the maximum of 100 iterations or when the relative change of the intensity $a_g^{(i)}$ is small, i.e. $|a_g^{(i)} - a_g^{(i-1)}|/|a_g^{(i)}| < 0.001$.

In order to see the performance, we choose two different trajectories: one is located in the pixels of the planet, and the other is in the same annulus and located in the pixels without a planet. Figure 1 shows how the flux a_g changes in each iteration. The results for both norms show that there is a considerable amount of change in the flux a_g for the P_g in the planet pixels, whereas the change in the flux a_g for the P_g in the pixels without a planet is very small.

In Fig. (2a, 2e) and Fig. (2b, 2f), we examine the performance of AMAT when testing a location without a planet. We see that the estimated flux is of

ESANN 2023 proceedings, European Symposium on Artificial Neural Networks, Computational Intelligence and Machine Learning. Bruges (Belgium) and online event, 4-6 October 2023, i6doc.com publ., ISBN 978-2-87587-088-9. Available from http://www.i6doc.com/en/.

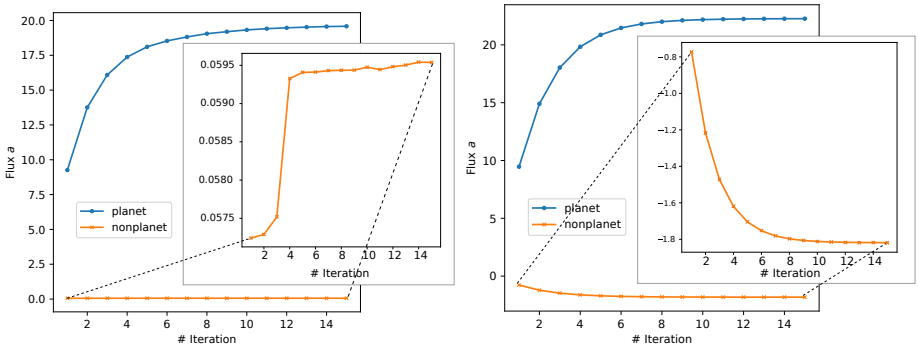

Fig. 1: Intensity a of the planet against the number of iterations. Left: The intensity $a_g^{(i)}$ is obtained using ℓ_1 norm. Right: The intensity $a_g^{(i)}$ is obtained using ℓ_2 (Frobenius) norm. The blue plots show how the intensity changes in each iteration when we choose P_g in the location of the planet. The orange plots show how the intensity changes in each iteration when we choose P_g in a location without a planet.

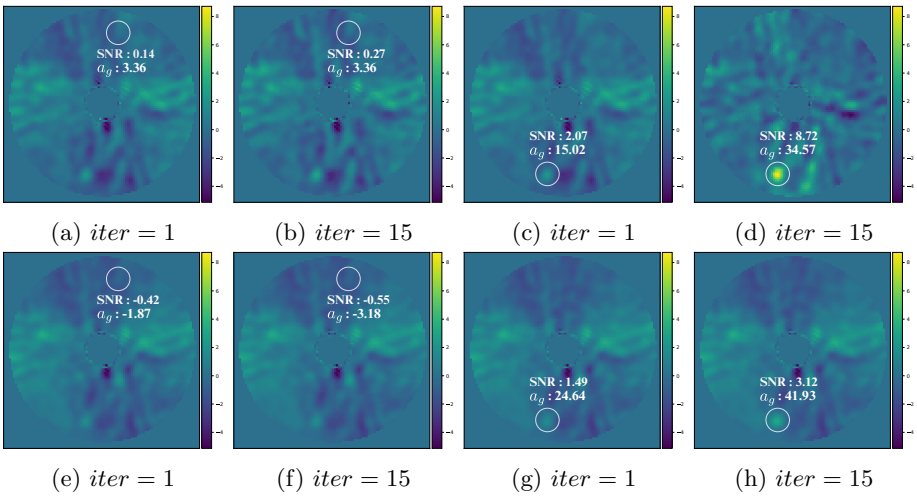

(a) $iter = 1$ (b) $iter = 15$ (c) $iter = 1$ (d) $iter = 15$

(e) $iter = 1$ (f) $iter = 15$ (g) $iter = 1$ (h) $iter = 15$

Fig. 2: Top: The SNR maps using ℓ_1 norm. Bottom: The SNR maps using Frobenius norm. Here, we apply SNR maps to the interim frame obtained by using only one P_g to show the performance of applying the algorithm with multiple iterations as a visual, but normally we apply SNR maps to the flux map obtained by combining all fluxes a_g. The white circle represents the location of P_g. Left two columns: P_g is located in the pixels without a planet. Right two columns: P_g is located in the planet pixels.

very small magnitude, and with additional iterations, this estimation does not change by much.

ESANN 2023 proceedings, European Symposium on Artificial Neural Networks, Computational Intelligence and Machine Learning. Bruges (Belgium) and online event, 4-6 October 2023, i6doc.com publ., ISBN 978-2-87587-088-9. Available from http://www.i6doc.com/en/.

In contrast, when AMAT is tested on a location with a planet in Fig (2c, 2g) and Fig (2d, 2h), we see that it detects the flux much more strongly, which gets more pronounced after the additional iterations.

When comparing the results for the ℓ_1 and ℓ_2 norms in Fig. 2, we see that, in general, the ℓ_1 estimator is able to produce a much better SNR at the price of solving a more challenging non-smooth optimization problem.

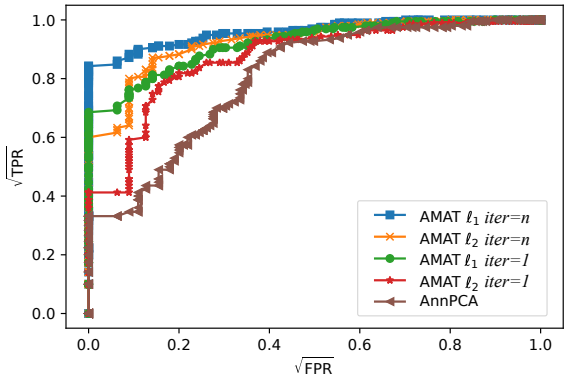

Fig. 3: ROC curves of algorithms. To better visualize the low false positive rate (FPR) regime, we adjust the scaling of the axes by taking their square root. The legend labels *iter=n* and *iter=1* represent the algorithm variants performing the maximum of 100 iterations and only a single iteration, respectively.

We calculate the deterministic ROC curves by following the approach outlined in [13], which involves counting the true positive (TPR) and false positive (FPR) detections. We produce ROC curves by generating synthetic groundtruth examples with the standard deviation of the pixel intensities in the annulus by injecting fake planets into a data cube without planets using the VIP package [7, 8]. In the context of exoplanet detection, the most relevant part of the ROC curve is in the low FPR regime. The plots in Fig. 3 demonstrate that our method consistently outperforms the results of AnnPCA and the variant performing just a single iteration in terms of ROC curves. Moreover, similar to the findings for the SNR map, the results obtained using the ℓ_1 norm are better than those obtained with the ℓ_2 norm.

4 Conclusion

In this paper, we propose a new AMAT method and demonstrate the benefit of estimating the flux and the low-rank quasi-static speckle components simultaneously. This is in contrast to most of the existing methods that perform the estimation of the two components sequentially. Applying our method on the locations with planets enhances the estimated flux, while keeping parts of the

ESANN 2023 proceedings, European Symposium on Artificial Neural Networks, Computational Intelligence and Machine Learning. Bruges (Belgium) and online event, 4-6 October 2023, i6doc.com publ., ISBN 978-2-87587-088-9. Available from http://www.i6doc.com/en/.

image with no planet relatively unchanged. Future work could delve into the consequences of iterative implementation in combination with other flux detection techniques, such as the likelihoodmap [13].

References

[1] Exoplanet catalog, NASA Exoplanet Exploration Program. `https://exoplanets.nasa.gov/discovery/exoplanet-catalog/`. Accessed: 5/5/2023.

[2] J-L Beuzit, A. Vigan, D. Mouillet, K. Dohlen, R. Gratton, A. Boccaletti, J-F Sauvage, H. M. Schmid, M. Langlois, C. Petit, et al. SPHERE: The exoplanet imager for the very large telescope. *Astronomy & Astrophysics*, 631:A155, 2019.

[3] J. R. Males, M. P. Fitzgerald, R. Belikov, and O. Guyon. The mysterious lives of speckles. I. residual atmospheric speckle lifetimes in ground-based coronagraphs. *Publications of the Astronomical Society of the Pacific*, 133(1028):104504, oct 2021.

[4] C. Marois, D. Lafreniere, R. Doyon, B. Macintosh, and D. Nadeau. Angular differential imaging: a powerful high-contrast imaging technique. *The Astrophysical Journal*, 641(1):556, 2006.

[5] A. Amara and S. P. Quanz. Pynpoint : An image processing package for finding exoplanets: Pynpoint. *Monthly Notices of the Royal Astronomical Society*, 427(2):948–955, December 2012.

[6] R. Soummer, L. Pueyo, and J. Larkin. Detection and characterization of exoplanets and disks using projections on Karhunen-Loève eigenimages. *The Astrophysical Journal*, 755(2):L28, August 2012.

[7] C. A. Gomez Gonzalez et al. VIP : Vortex Image Processing Package for High-contrast Direct Imaging. *The Astronomical Journal*, 154(1):7, June 2017.

[8] V. Christiaens, C. Gonzalez, R. Farkas, C.-H. Dahlqvist, E. Nasedkin, et al. VIP: A Python package for high-contrast imaging. *The Journal of Open Source Software*, 8(81):4774, January 2023.

[9] C. A. Gomez Gonzalez et al. Low-rank plus sparse decomposition for exoplanet detection in direct-imaging ADI sequences: The LLSG algorithm. *Astronomy & Astrophysics*, 589:A54, May 2016.

[10] S. Vary, H. Daglayan, L. Jacques, and P.-A. Absil. Low-rank plus sparse trajectory decomposition for direct exoplanet imaging. *arXiv preprint arXiv:2301.07018*, 2023. in press.

[11] H. Daglayan, S. Vary, V. Leplat, N. Gillis, and P.-A. Absil. Direct exoplanet detection using l1 norm low-rank approximation. *arXiv preprint arXiv:2304.03619*, 2023.

[12] C.-H. Dahlqvist, F. Cantalloube, and O. Absil. Regime-switching model detection map for direct exoplanet detection in ADI sequences. *Astronomy & Astrophysics*, 633:A95, 2020.

[13] H. Daglayan, S. Vary, F. Cantalloube, P.-A. Absil, and O. Absil. Likelihood ratio map for direct exoplanet detection. In *2022 IEEE 5th International Conference on Image Processing Applications and Systems (IPAS)*, volume 5, pages 1–5, 2022.

[14] D. Mawet, J. Milli, Z. Wahhaj, D. Pelat, O. Absil, C. Delacroix, A. Boccaletti, M. Kasper, M. Kenworthy, C. Marois, B. Mennesson, and L. Pueyo. FUNDAMENTAL LIMITATIONS OF HIGH CONTRAST IMAGING SET BY SMALL SAMPLE STATISTICS. *The Astrophysical Journal*, 792(2):97, aug 2014.